

SCIENTIFIC REPORTS



OPEN

Biochemical and Structural Analysis of a Novel Esterase from *Caulobacter crescentus* related to Penicillin-Binding Protein (PBP)

Received: 22 July 2016
Accepted: 03 November 2016
Published: 01 December 2016

Bum Han Ryu^{1,2,*}, Tri Duc Ngo^{2,*}, Wanki Yoo^{1,2}, Sojeong Lee¹, Boo-Young Kim¹, Euijoo Lee¹, Kyeong Kyu Kim² & T. Doohun Kim¹

Considering that the prevalence of antibiotic-resistant pathogenic bacteria is largely increasing, a thorough understanding of penicillin-binding proteins (PBPs) is of great importance and crucial significance because this enzyme family is a main target of β -lactam-based antibiotics. In this work, combining biochemical and structural analysis, we present new findings that provide novel insights into PBPs. Here, a novel PBP homologue (CcEstA) from *Caulobacter crescentus* CB15 was characterized using native-PAGE, mass spectrometry, gel filtration, CD spectroscopy, fluorescence, reaction kinetics, and enzyme assays toward various substrates including nitrocefin. Furthermore, the crystal structure of CcEstA was determined at a 1.9 Å resolution. Structural analyses showed that CcEstA has two domains: a large α/β domain and a small α -helix domain. A nucleophilic serine (Ser⁶⁸) residue is located in a hydrophobic groove between the two domains along with other catalytic residues (Lys⁷¹ and Try¹⁵⁷). Two large flexible loops (UL and LL) of CcEstA are proposed to be involved in the binding of incoming substrates. In conclusion, CcEstA could be described as a paralog of the group that contains PBPs and β -lactamases. Therefore, this study could provide new structural and functional insights into the understanding this protein family.

The bacterial cell wall is composed of polymeric glycan chains with alternating N-acetylglucosamine (NAG) and N-acetylmuramic acid (NAM), which are crosslinked by short peptide branches^{1–3}. This peptidoglycan layer forms the major structural component of the protective barrier and disruption of these layer leads to bacterial cell lysis. Penicillin-binding proteins (PBPs) are a large group of periplasmic enzymes that catalyze essential functions in the synthesis, modification, and maintenance of these peptidoglycans^{4–5}. PBPs are responsible for two unique enzymatic activities; transglycosylation to form the glycan backbone by polymerizing disaccharides, and transpeptidation to catalyze cross-linking between adjacent glycan chains to create a mesh-like structure. In addition, PBPs are the targets of β -lactam antibiotics including penicillin and cephalosporin, which bind to the active site of PBPs as structural homologs of D-alanyl-D-alanine^{6–7}.

Penicillin-binding proteins (PBPs) are classified into high-molecular-weight (HMW) PBPs and low-molecular-weight (LMW) PBPs based on molecular weight and sequence homology. HMW PBPs are responsible for peptidoglycan polymerization, cross-linking, and insertion of the peptidoglycan precursors into the preexisting strands through transglycosylation and transpeptidation reactions. HMW PBPs can catalyze both the polymerization of a peptidoglycan from disaccharide peptides (transglycosylase) and the cross-linking of muramyl peptides (transpeptidase). HMW PBPs are divided into subclass A and subclass B, which are bifunctional transpeptidases/transglycosylases (subclass A) and monofunctional transpeptidases (subclass B), respectively. The low-molecular-weight (LMW) PBPs have only the transpeptidase (TP) domain that catalyzes carboxypeptidase and endopeptidase activity *in vitro*, which play a role in peptidoglycan maturation.

¹Department of Chemistry, College of Natural Science, Sookmyung Women's University, Seoul 140-742, Korea.

²Department of Molecular Cell Biology, Samsung Biomedical Research Institute, Sungkyunkwan University School of Medicine, Suwon, 440-746, Korea. *These authors contributed equally to this work. Correspondence and requests for materials should be addressed to K.K.K. (email: kyeongkyu@skku.edu) or T.D.K. (email: doohunkim@sookmyung.ac.kr)

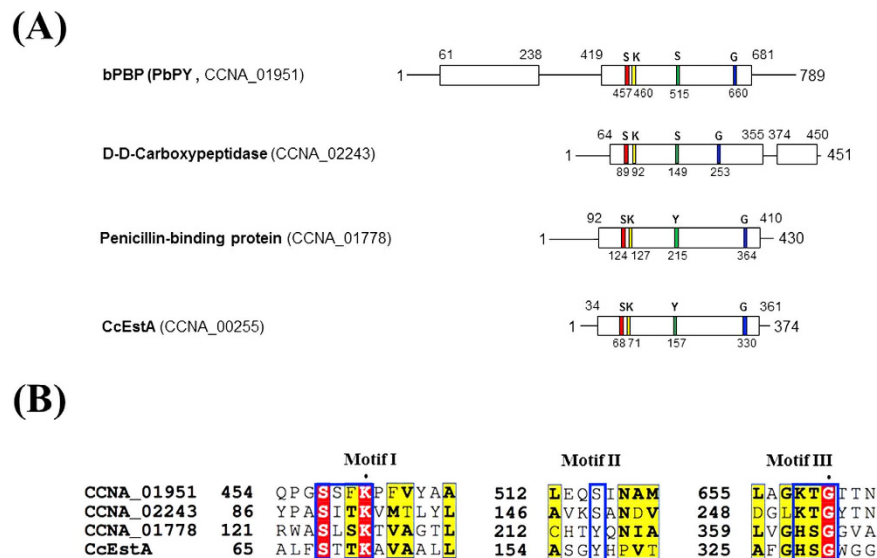


Figure 1. Overall structural organization and multiple sequence alignment of CcEstA. (A) The structural organization of CcEstA is compared with other related proteins in *Caulobacter crescentus*. Note that important catalytic residues (colored residues) are highly conserved and lie on spatially similar positions in each protein. (B) Multiple sequence alignment of CcEstA was performed with related proteins in *C. crescentus* using *Clustal Omega* and *ESPrpt*. Only three characteristic motifs of these proteins (motif I, II and III) are shown for clarity and highly conserved residues are shown in red.

Caulobacter crescentus, an important prokaryote for studying cellular differentiation and asymmetric division, is a widespread Gram-negative bacterium that has two distinct life stages; a motile swarmer cell and a sessile stalked cell^{8–9}. Recently, it has been shown that PBPs in *C. crescentus* can interact with the cell wall synthetic complexes for cell elongation or stalk growth, facilitating the independent regulation of distinct growth processes^{10–11}. However, biochemical studies of PBPs or their homologs in this microbe are largely unknown, and our understanding about their molecular structures and catalytic mechanism is still limited.

Recently, a number of bacterial enzymes with high similarities to PBPs have been identified from metagenomics libraries. These include EstU1¹², Est22¹³, EstM-N1¹⁴, and EstC¹⁵. In a previous study, identification and preliminary X-Ray diffraction analysis of a novel PBP homolog (CcEstA, CCNA_00255) in *Caulobacter crescentus* CB15 were reported¹⁶. CcEstA was shown to catalyze the hydrolysis of industrially important compounds including ketoprofen ethyl ester. Here, biochemical and structural analysis of CcEstA were performed, which could pave a way for understanding the structure and function of PBP family proteins.

Results and Discussion

Sequence analysis of CcEstA. The primary sequence of CcEstA is composed of a single polypeptide chain with 374 amino acids. Sequence analysis showed that CcEstA shared some sequence identity with D-Ala-D-Ala transpeptidase from *Streptomyces sp.* R61 (16.5%, P15555), and *Bacillus halodurans* (14.5%, P32959), and with β -lactamases from *Ochrobactrum anthropi* SV3 (14.0%, Q9ZBA9) and *Enterobacter cloacae* (16.0%, P05364). In protein databases, similar sequences to CcEstA were mainly annotated as members of the PBP or transpeptidase (TP) superfamilies. All PBPs or their homologs are believed to contain three characteristic motifs (Motifs I, II, and III), which are involved in catalysis^{4,6,17}. These motifs are highly conserved with similar spacing along the polypeptides, which suggests a common evolutionary origin^{18,19}. In addition, similar motifs and residues are also found in DD-peptidase²⁰ and D-amino acid amidase²¹. Three sequence motifs (motif I, II, and III) of CcEstA have been identified through sequence comparisons with other PBP family proteins. Motif I typically includes a catalytic serine residue in the tetra-peptide of SxxK. In the case of CcEstA, a nucleophilic Ser⁶⁸ is indeed found in the characteristic tetrapeptide, S⁶⁸-x-x-K⁷¹. In this motif, Ser acts as a nucleophile, while Lys is involved in the acylation step as a general base. The key residue of motif II is a Tyr or Ser, the hydroxyl group of which is involved in activating and deacylating the nucleophilic Ser⁷. Interestingly, unlike other two motifs, motif III is not strictly conserved in the PBP family or its homolog proteins. In the case of CcEstA, His³²⁸-Ser³²⁹-Gly³³⁰ is found in motif III, whereas other closely-related proteins contains highly conserved Lys(K)-Thr(T)-Gly(G) motif at the same position. Therefore, only a glycine among these three residues is conserved. As shown in Fig. 1, CcEstA has similar catalytic residues to the TP domains in bifunctional penicillin-binding protein (PbpY, CCNA_01951), DD-carboxypeptidase (CCNA_02243), and penicillin binding protein (CCNA_01778) in the chromosome of *Caulobacter crescentus*. Taken together, multiple sequence alignment suggests that CcEstA shares sequence similarity with PBPs or the TP domain of bPBPs, suggesting that they all share common features in their functions and structures.

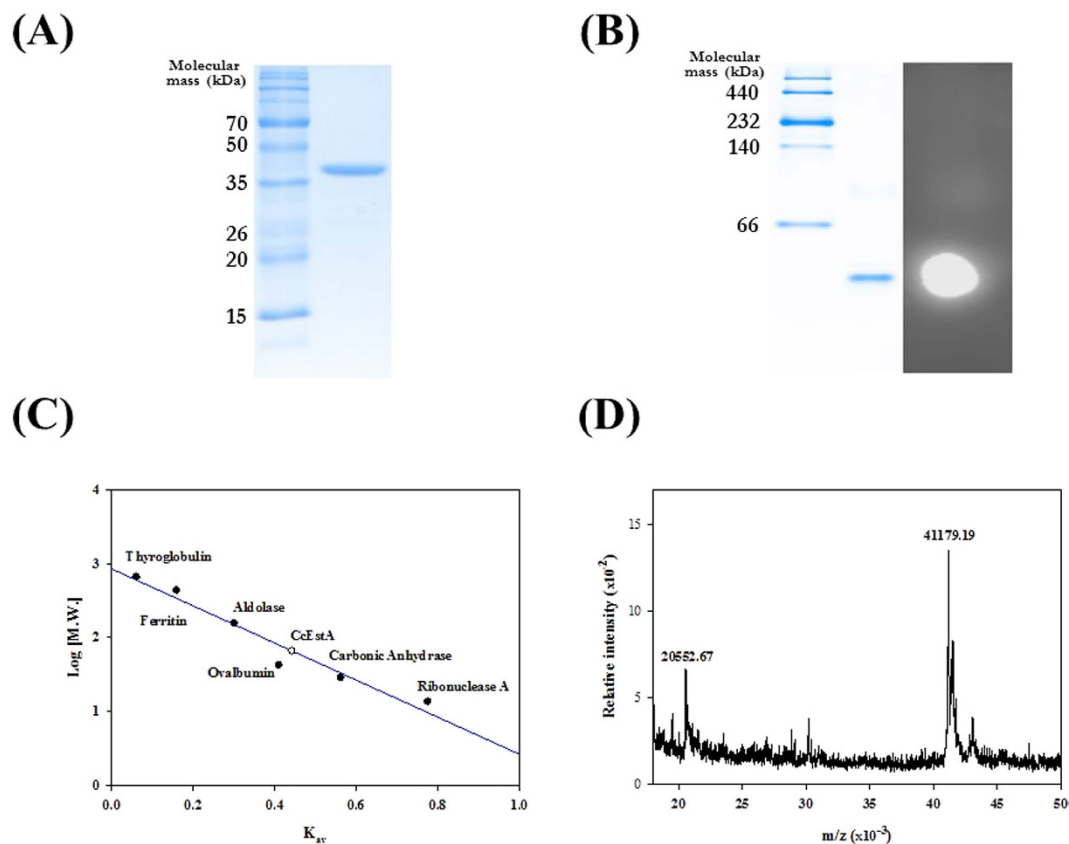


Figure 2. Characterization of CcEstA. (A) Purified CcEstA was analyzed by SDS-PAGE and then stained with Coomassie Brilliant Blue (*left*; molecular standards marker, *right*; purified CcEstA). (B) Native-PAGE analysis with 4-MU overlay assay of CcEstA. Only one band appears on Native-PAGE gel (*left*) showing the fluorescent signal from 4-MU catalysis (*right*). (C) Size exclusion chromatography of CcEstA under non-denaturing conditions. (D) MALDI-TOF mass spectrum of CcEstA. The $[M+H]^+$ and $[M+2H]^{2+}$ ion peaks were found at m/z value of 20,552, and 41,179, respectively.

Biochemical characterization of CcEstA. The recombinant CcEstA was purified to near-homogeneity, and a single band with a molecular mass of ~37 kDa was observed after Coomassie brilliant blue (CBB) staining (Fig. 2A). An overlay activity assay with 4-methylumbelliferyl (4-MU) acetate as a substrate showed high fluorescence due to the formation of 4-methylumbelliferone in native PAGE^{22,23}. In zymogram analysis, the molecular mass of active CcEstA is smaller than 66 kDa, implying that CcEstA is monomeric conformation (Fig. 2B). A similar behavior indicating a monomeric state in solution was also observed in size exclusion chromatography (Fig. 2C). Therefore, CcEstA seems to function as a monomer, which is consistent with other recently reported PBP structures^{24–26}. This is further supported by the fact that there are no expected dimeric interfaces within CcEstA as determined by the PISA program²⁷. Furthermore, Maldi-tof mass spectrometric analysis showed a major peak (m/z) at 41.1 kDa, which is consistent with the calculated molecular mass of recombinant CcEstA (Fig. 2D).

The substrate specificity of CcEstA was assessed using *p*-nitrophenyl esters with different acyl chain lengths²⁸. As shown in Fig. 3A, CcEstA showed a strong preference toward short-chain substrates such as *p*-nitrophenyl acetate (*p*-NA; C2) and *p*-nitrophenyl butyrate (*p*-NB; C4). However, less than 30% of initial enzyme activity was detected when longer chain substrates of *p*-nitrophenyl octanoate (*p*-NO; C8) or *p*-nitrophenyl decanoate (*p*-ND; C10) were used. No enzyme activity was noticed toward *p*-nitrophenyl phosphate (*p*-NP). Similarly, EstU1, Est22, EstM-N1 or EstC showed substrate preference for *p*-nitrophenyl butyrate (C4), while no enzyme activities of these enzymes was observed for *p*-nitrophenyl esters with longer chains (from C12 to C18)^{12–15}. When diverse naphthyl derivatives were used as substrates, the highest activities were obtained with 2-naphthyl acetate (2-NA), followed by 1-naphthyl acetate (1-NA), and 1-naphthyl butyrate (1-NB). In contrast, CcEstA showed very little activity toward 1-naphthyl phosphate (1-NP). The deacetylation activity of CcEstA towards various acetylated substrates showed that the highest activities were obtained with 2-naphthyl acetate (2-NA), followed by *p*-nitrophenyl acetate (*p*-NA) (Fig. S4).

For assessing thermostability of CcEstA, residual activity during the incubation of CcEstA at temperature ranges at 20–60 °C was monitored at 15 min intervals for 60 min. As shown in Fig. 3C, CcEstA was very stable up to 40 °C. However, at 50 °C, CcEstA lost its activity very rapidly and retained only ~25% of initial activity after 30 min. No enzyme activity was observed at 60 °C. To determine the optimum pH for CcEstA, enzyme activity was monitored at pH values from 3.0 to 10.0 (Fig. 3D). Although CcEstA was unstable in acidic environments, it

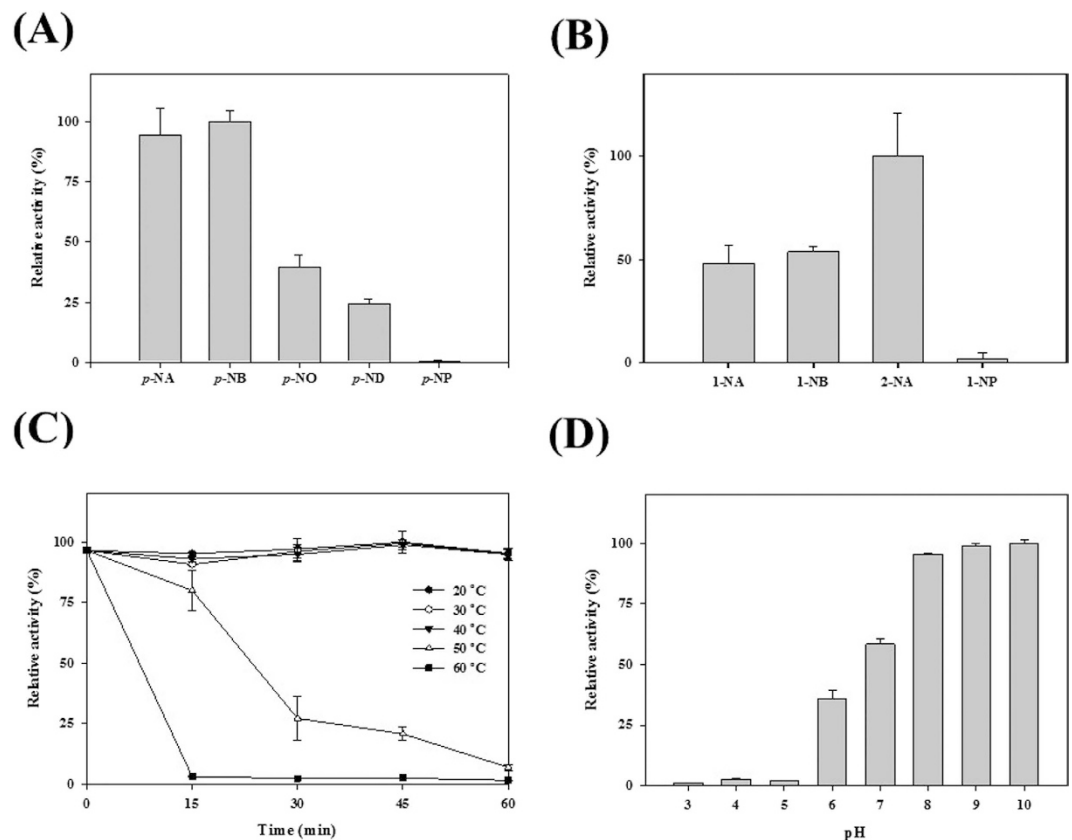


Figure 3. Enzyme assays of CcEstA. (A) Substrate-specificity assay of CcEstA using *p*-nitrophenyl esters with different acyl chain lengths. (B) Regioselectivity assay of CcEstA using naphthyl derivatives. (C) Activity of CcEstA in various temperatures from 20 to 60 °C for 1 h. (D) Activity of CcEstA in different pH solutions from pH 3 to 10.

was highly stable at alkaline pH values from 8.0 to 10.0, retaining almost maximum activity. At pH 7.0, only ~50% of the initial activity at pH 9.0 was observed. This behavior was also observed in EstU1¹² or EstM-N1¹⁴, which was highly stable at an alkaline pH of 9.0.

The structural stability of CcEstA in terms of thermal and chemical unfolding was investigated by circular dichroism (CD) and intrinsic fluorescence analysis, respectively²⁹. Subsequent far-UV CD spectra analysis revealed that CcEstA retains its stable conformation up to 40 °C without any significant structural changes. Above 50 °C, CD spectra showed increased values from 210 to 230 nm region, which is consistent with the results of enzyme activity assays (Fig. 4A). To determine the melting point, CD signals of CcEstA were monitored at 222 nm in temperatures from 20 to 60 °C. Remarkable structural transitions were observed around 50 °C (Fig. 4B). Chemical unfolding of CcEstA was monitored upon the addition of urea as determined by changes in intrinsic fluorescence (Fig. 4C). Without urea, native CcEstA exhibited a λ_{\max} of 349 nm and red shift of λ_{\max} to 364 nm was observed with a significant decrease of fluorescence intensity after the addition of 3 M urea. Additionally, CcEstA showed very little activity at concentrations of 3 M urea and above (Fig. 4D).

As shown in Fig. 5A, CcEstA exhibited hyperbolic Michaelis-Menten kinetics for three different substrates (*p*-NA, *p*-NO, and nitrocefin). From the values of kinetic parameters, catalytic efficiency (k_{cat}/K_m) for *p*-NA hydrolysis is about 1.25-fold higher than observed for *p*-NO hydrolysis (Fig. 5B). Interestingly, CcEstA showed significantly different kinetic parameters for nitrocefin with approximately a 27-fold higher K_m (1348 μM) and a 1880-fold lower k_{cat} (0.00807 s^{-1}) compared to *p*-NA. Therefore, compared with the *p*-NA or *p*-NO, the catalytic efficiency for nitrocefin was very low, revealing that CcEstA is more efficient on *p*-nitrophenyl esters than nitrocefin.

The chemical stability of CcEstA was also assessed with various kinds of detergents and organic solvents. As shown in Fig. 6A, CcEstA was stable in 10% ethanol (EtOH) without any loss of activity. Furthermore, it could retain over 60% of its initial activity in 1% Triton X-100 (TX-100) or 1% Tween 20 (Tw-20). For enantioselectivity analysis, a pH-drop colorimetric assay was used with (*R*)- and (*S*)-methyl- β -hydroxyisobutyrate³⁰. Following incubation with CcEstA, the reaction mixture containing the (*R*)-enantiomer turned yellow more rapidly, indicating the (*R*)-selectivity of CcEstA (Fig. 6B). The ability of CcEstA to hydrolyze tertiary alcohol esters (TAEs) was examined using *tert*-butyl acetate, α -terpinyl acetate, and linalyl acetate as substrates²⁸. As shown in Fig. 6C, CcEstA hydrolyzed *tert*-butyl acetate, linalyl acetate, and the bulky α -terpinyl acetate. A pH-indicator-based colorimetric assay based upon the release of acetic acid was employed. As shown in Fig. 6C, CcEstA hydrolyzed *tert*-butyl acetate, α -terpinyl acetate, and linalyl acetate. Considering the fact that tertiary alcohols are

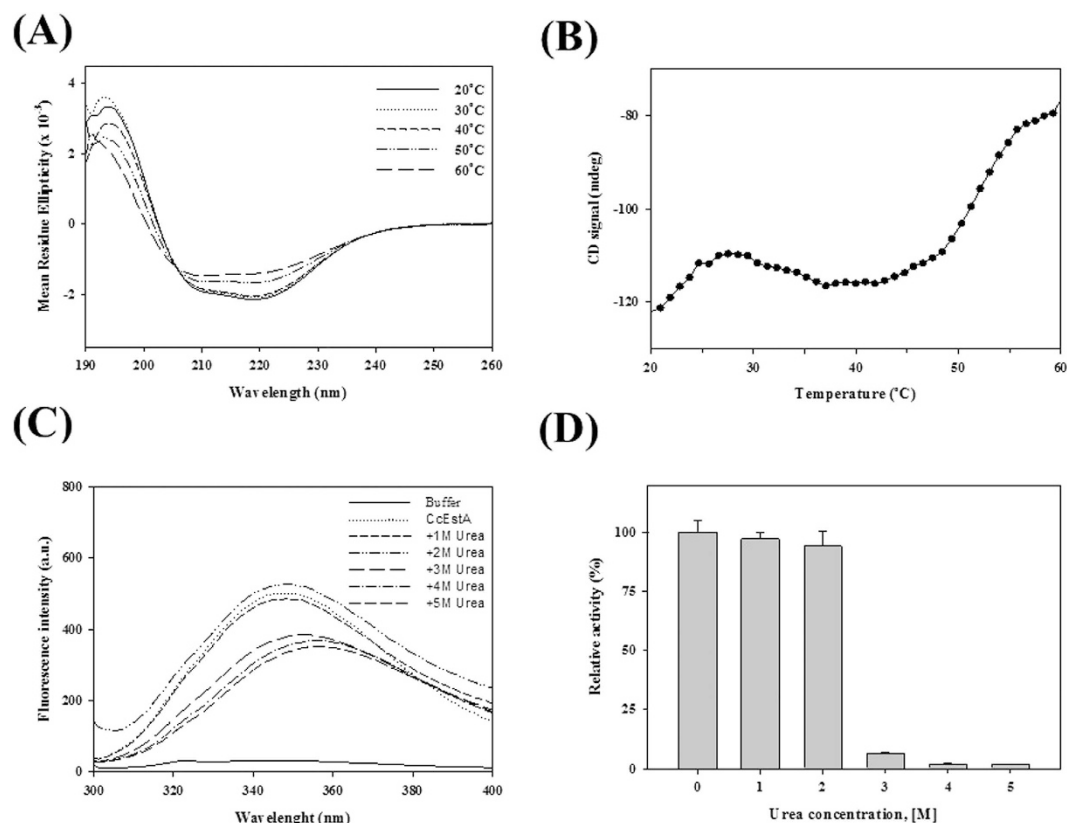


Figure 4. Structural stability of CcEstA. (A,B) Thermal analysis of CcEstA was monitored in various temperature from 20 to 60 °C using circular dichroism spectrometry (A; from 190 to 260 nm, B; at 222 nm). Note that CcEstA undergoes notable changes in structure above 50 °C. (C,D) Chemical unfolding of CcEstA. Intrinsic fluorescence spectra (C) and relative enzyme activity of CcEstA with various concentrations of urea from 0 to 5 M were recorded after 1 h incubation (D).

expensive building blocks in the pharmaceutical industry³¹, CcEstA could be used as a biocatalyst for industrial applications. Additionally, to investigate the β -lactamase activity of CcEstA, a chromogenic β -lactamase substrate (nitrocefin) was used as a substrate³². As shown in Fig. 6D, CcEstA apparently showed β -lactamase activity toward nitrocefin, which was verified with the color change of the reaction mixture. The β -lactamase activity of CcEstA was further investigated using 7-ACA and CTX (Fig. 7A). Compared to PBS-2, CcEstA showed no catalytic activities towards 7-aminocephalosporanic acid (7-ACA) or cefotaxime (CTX) as determined by a pH shift assay (Fig. 7B). Furthermore, both 7-ACA and CTX had almost no inhibitory effects toward nitrocefin hydrolysis by CcEstA (Fig. 7C), implying that the substrate-binding site of CcEstA is not suitable for 7-ACA or CTX. In this respect, the absence of N in the S(Y)xN motif could be related to the relatively low activity of CcEstA towards β -lactam compounds because this N is usually employed in hydrogen bonding to β -lactam side chain amide groups⁴⁻⁶. In accordance with CcEstA, EstC and EstM-N1 have shown significant hydrolyzing activity for nitrocefin, but did not display activity for β -lactam substrates. However, EstU1 and Est22 were shown to possess a significant β -lactam hydrolytic activity for cephalosporin derivatives.

Overall Structure of CcEstA. The crystal structure of CcEstA that belongs to the $P2_12_12_1$ space group was determined at a 1.9-Å resolution with R_{work} of 17.04% ($R_{\text{free}} = 20.10\%$). The crystallographic statistics for data collection and structure refinement are summarized in Table 1. Although most residues of CcEstA are well-defined, residues located in positions 237 to 239 were not visible in the final $2F_o - F_c$ electron density map. In many PBP structures, disorders of similar loop regions are observed^{32,33}. A Ramachandran plot revealed that all residues are in the most favored and additionally allowed regions (data not shown). The overall structure of CcEstA consisted of two domains: a large α/β domain and a small α domain (Fig. 8A), which is also found in other PBPs and serine β -lactamases³⁴. The large α/β domain (residue 1–85 and 175–374) has a seven-stranded anti-parallel β -sheet ($\beta_2, \beta_1, \beta_7, \beta_6, \beta_5, \beta_4$, and β_3) enclosed by six helices ($\alpha_2, \alpha_7, \alpha_8, \alpha_9, \alpha_{10}$, and α_{11}) on one face and two helices (α_1 and α_{12}) on the other face (Fig. 8B). The small α domain (residue 86–174) includes four helices ($\alpha_3, \alpha_4, \alpha_5$, and α_6). These two domains create a deep hydrophobic tunnel in which the catalytic serine is located 8.5 Å near the bottom of the cleft (Fig. 8C). The four residues (S⁶⁸-T⁶⁹-T⁷⁰-K⁷¹) in Motif I are found at the N-terminal end of α_2 helix. Tyr¹⁵⁷ of Motif II lies on the loop between α_5 and α_6 helices. Histidine (His³²⁸) and glycine (Gly³³⁰) of Motif III are situated at the C-terminal end of β_6 . Figure 8D shows the electrostatic surface of CcEstA, highlighting the positive charges of many arginine and lysine residues present in the large α/β domain. Specifically,

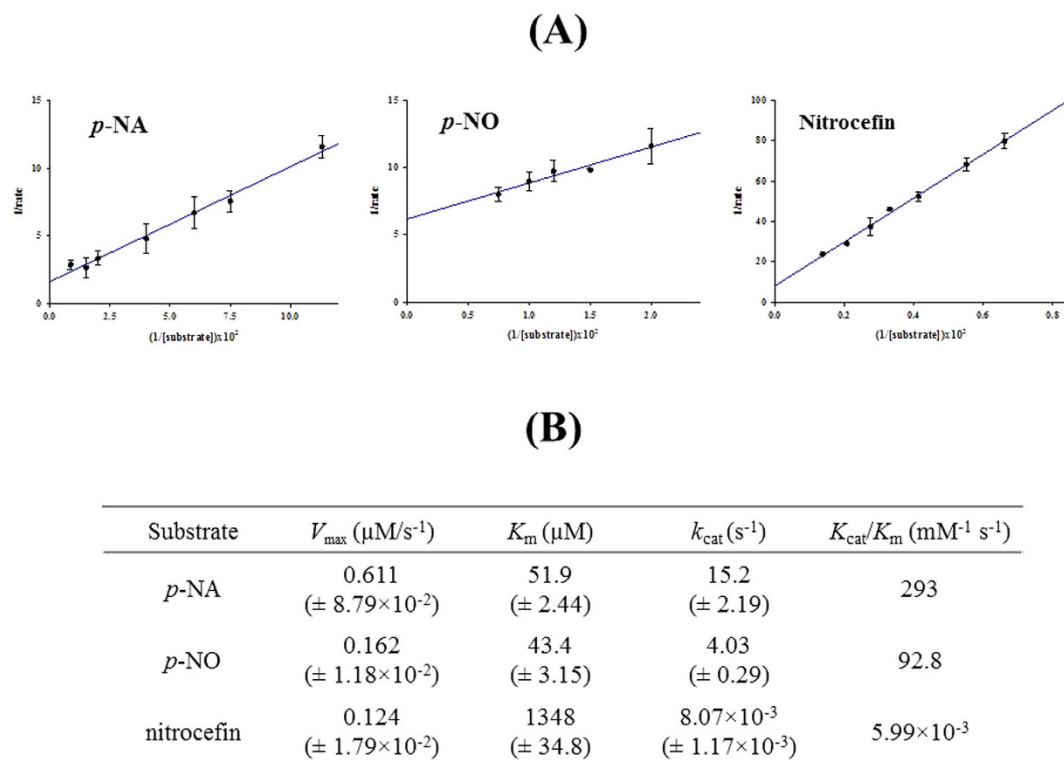


Figure 5. Kinetics analysis of CcEstA. With three different substrates (*p*-nitrophenyl acetate; *p*-NA, *p*-nitrophenyl octanoate; *p*-NO, and nitrocefin), V_{\max} , K_m , and k_{cat} of CcEstA were determined from the Lineweaver-Burk plot. Standard errors for the parameters are shown in parenthesis.

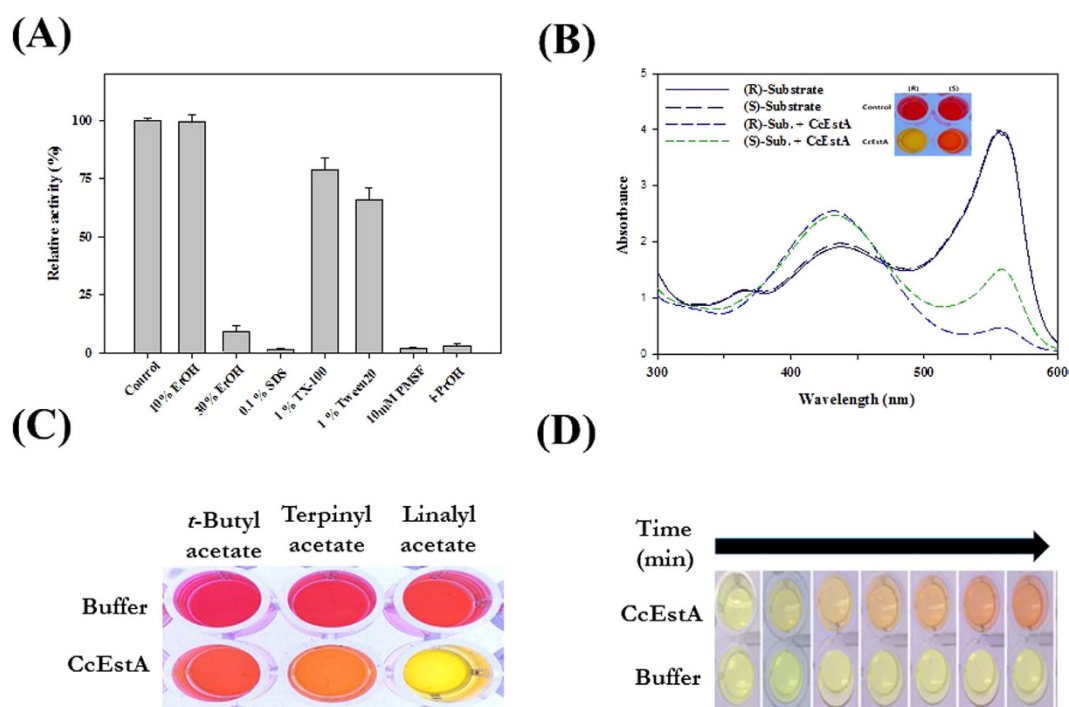


Figure 6. Biochemical analysis of CcEstA. (A) Chemical stabilities of CcEstA. The residual activities of CcEstA after 1 h incubation with different solvents are expressed relative to the initial activity (100%). (B) pH shift assay was performed to assess the enantioselectivity of CcEstA toward (*R*)- and (*S*)- methyl-3-hydroxy-2-methylpropionate. (C) Tertiary alcohol production by CcEstA using *tert*-butyl acetate, α -terpinyl acetate and linalyl acetate (LA). (D) β -lactamase activity of CcEstA using nitrocefin.

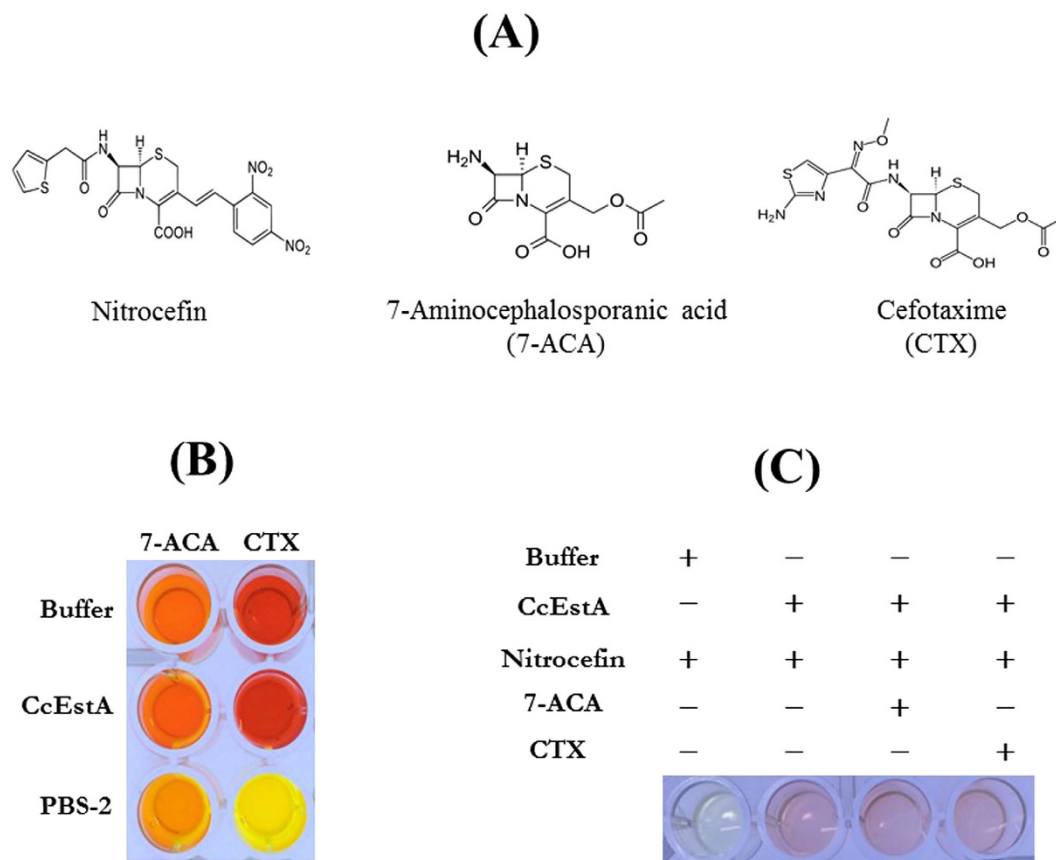


Figure 7. Hydrolytic activity of CcEstA toward β -lactam-related compounds. (A) Chemical structures of nitrocefin, 7-aminocephalosporanic acid (7-ACA), and cefotaxime (CTX). (B) A pH shift assay was conducted to verify the hydrolytic activity of CcEstA toward 7-ACA and CTX. PBS-2, a bacterial PBP homologue from *Paenibacillus sp.*, was used as a positive control⁵⁵. Note that CcEstA showed almost no hydrolytic activity toward 7-ACA and CTX, while nitrocefin can be hydrolyzed. (C) Competitive inhibition assay of CcEstA. 7-ACA and CTX were used as competitive inhibitors of nitrocefin. Note that both 7-ACA and CTX have almost no inhibitory effect on nitrocefin hydrolysis.

a cluster of aspartic acids (Asp¹²⁸, Asp¹³⁴, and Asp¹³⁶) and glutamic acid (Glu¹²⁶) are observed in the small α domain, which are highly conserved in other related PBPs.

The domain-domain interactions of CcEstA are mainly composed of residues from $\alpha 2$, $\alpha 4$, $\alpha 6$, and $\beta 4$ with residues from three loops ($\alpha 2/\alpha 3$, $\alpha 4/\alpha 5$, $\alpha 5/\alpha 6$, $\alpha 6/\alpha 7$ loop, $\alpha 8/\alpha 9$ loop, and $\beta 4/\beta 5$ loop), which include salt-bridges of Arg¹⁷⁶ (on the loop between $\alpha 6$ and $\alpha 7$) – Asp¹⁷⁴ (on the loop between $\alpha 6$ and $\alpha 7$) and Arg²⁹² (on $\beta 4$) – Glu¹¹¹ (on $\alpha 4$). Extensive hydrogen bonding networks were also formed including Lys⁷¹, Leu⁸¹, Val⁸², Gly¹⁷⁵, Arg¹⁷⁶, Trp²³³, Arg²⁹², and Asp²⁹⁷, and Leu²⁹⁸ of the large α/β domain and Gly⁸⁵, Arg⁸⁶, Leu⁸⁷, Glu¹¹¹, Phe¹²³, Trp¹³², Ser¹⁵⁵, Tyr¹⁵⁷, Pro¹⁵⁹, Tyr¹⁶², Arg¹⁷¹, and Asp¹⁷⁴ of the small α domain (Fig. 9A). The active site of CcEstA is located in the cleft at the interface between the α/β domain and the small α domain, which is lined by a series of highly conserved residues. The active site of CcEstA shows a compact hydrogen-bonding network around catalytic residues to activate Ser⁶⁸ for the acylation step (Fig. 9B). Specifically, Lys⁷¹-N ζ forms hydrogen bonds with the O γ of Ser⁶⁸ (2.6 Å), O η of Tyr¹⁵⁷ (2.9 Å), and the carbonyl group of Pro¹⁵⁹ (2.8 Å) and Ser²⁵¹ (3.0 Å). An amide group of Lys⁷¹ is also involved in a hydrogen-bonding network with a carbonyl group of Ser⁶⁸ and O γ of Ser⁶⁸ was found to be spatially separated from O η of Tyr¹⁵⁷ by 2.7 Å. Therefore, O γ of Ser⁶⁸ forms two hydrogen bonds to N ζ of Lys⁷¹ and O γ of Ser⁶⁸.

To compare CcEstA to other homologous proteins, DALI and BLAST searches were executed with available structures in the Protein Data Bank (PDB). CcEstA showed structural similarity to R61 DD-peptidase (PDB ID: 3PTE, Z-score 28.8) from *Streptomyces* R61, with root-mean-square deviations (RMSD) of 2.68 Å for 279 C α atoms. Furthermore, CcEstA also showed structural similarity to a PBP from *Pyrococcus abyssi* (PaPBP, PDB ID: 2QMI, Z-score 30.0), with an RMSD of 2.46 Å for 288 C α atoms. These two enzymes have 15.2 and 12.6% sequence identity with CcEstA, respectively, and only 34 residues are completely conserved among these enzymes (Fig. S1). The structural comparison of CcEstA with R61 DD-peptidase and PaPBP revealed that catalytic residues are completely conserved among these enzymes. Locations of Ser⁶⁸, Lys⁷¹, Tyr¹⁵⁷, and His³²⁸ in CcEstA are structurally equivalent to those of R61 DD-peptidase and PaPBP (Fig. 10A). Furthermore, the spatial locations of glycine in Motif III of CcEstA (Gly³³⁰), involved in oxyanion hole formation, are similar to those of R61

	EstCC
Data collection	
Space group	$P2_12_12_1$
Cell dimensions	
a, b, c (Å)	58.277
	67.308
	92.093
α, β, γ (°)	90, 90, 90
Molecules/AU	1
Wavelength	0.919805
Resolution (Å)	50–1.90
No. reflections	29140
R_{sym} or R_{merge}^1	10.7 (37.9)
Mean $(I/\sigma I)$	34.8 (5.3)
Completeness (%)	99.9 (100)
Redundancy	7.2 (7.3)
Refinement	
Resolution (Å)	30–1.9
No. reflections	28932
$R_{\text{work}}^2/R_{\text{free}}^3$	17.04/20.10
No. atoms	
Protein	2801
Ligand/ion	—
Water	348
B -factors	
Protein	21.24
Ligand/ion	—
R.M.S.D ⁴	
Bond lengths (Å)	0.007
Bond angles (°)	0.857
Ramachandran statistics ⁵ (%)	97.28/2.72/0.00
Completeness (%)	99.9 (100)

Table 1. Data collection and refinement statistics for CcEstA structure. (Values in parentheses refer to the last resolution shell). ¹ $R_{\text{symm}}(\%) = \frac{\sum_h \sum_i |I(h_i) - \langle I(h) \rangle|}{\sum_h \sum_i I(h_i)}$, where $I(h_i)$ is the single intensity of reflection h as determined by the i th measurement and $\langle I(h) \rangle$ is the mean intensity of reflections h . ² $R_{\text{cryst}}(\%) = \frac{\sum |Fo - Fc|}{\sum Fo}$, where, Fo is the observed structure factor amplitude, and Fc is the structure factor calculated from the model. ³ $R_{\text{free}}(\%)$ is calculated in the same manner as R_{cryst} using 5% of all reflections excluded from refinement stages using high resolution data. ⁴R.M.S.D., Root-mean-square deviation. ⁵The fraction of residues in the favored, allowed, and disallowed regions of the Ramachandran diagram calculated by MOLPROBITY.

DD-peptidase (Gly³³¹) and PaPBP (Gly³³⁷) (Fig. S1). In addition, the area of domain-domain interface of CcEstA (1720 Å²) is similar to that of PaPBP (1778 Å²), but larger than that of R61 DD-peptidase (1406 Å²). Interestingly, significant differences were observed in the size and shape of their substrate-binding pockets (Fig. 10B).

Substrate-binding pocket of CcEstA. In previous reports, size and shape of the substrate-binding pocket are shown to affect substrate specificity of PBPs²⁰, DD-peptidase³⁵, and D-amino acid amidase²¹. Using CASTp server, the substrate-binding pocket of CcEstA was compared to that of homologous proteins. Interestingly, CcEstA showed a moderate pocket area (371.2 Å²) and volume (267.8 Å³) comparable to those of R61 DD-peptidase (203.80 Å², 229.0 Å³). However, the pocket area and volume of PaPBP (1184.5 Å², 1963.7 Å³) are relatively larger than the other two enzymes. In CcEstA, the upper end of the substrate-binding pocket is delineated by $\alpha 8$, $\alpha 9$, $\alpha 8/\alpha 9$, and $\alpha 9/\alpha 10$ including Val¹⁶⁰, Ser²³⁴, Ser²³⁵, Pro²³⁶, and Trp²⁴⁴, Ile²⁴⁹, Ser²⁵¹, and Ala²⁵², with the side chains of Phe⁶⁷ and Pro¹⁵⁹ forming a roof over the cleft (Fig. 11A). The Gly³²⁷-His³²⁸-Ser³²⁹-Gly³³⁰ motif was attached to the side end of the cleft through a short strand $\beta 5$, and the indole ring of Trp³³¹ was inserted into the active site. The $\alpha 5/\alpha 6$ and $\beta 3/\beta 4$ loops as well as Leu³⁰⁰ and Trp³⁰⁶ lay along one side of the substrate-binding cleft to form a wall with the $\beta 5/\beta 6$ loop forming the opposite wall. Furthermore, Ser²⁵¹ and Ala²⁵² together form part of the substrate-binding pocket of CcEstA and Pro¹⁵⁹, Val¹⁶⁰, Ile²⁴⁹, His³²⁸, and Ser³²⁹ are involved in the hydrogen-bonding network of this region. As shown in Fig. 11A, Phe⁶⁷ and Trp³³¹ take one side of the wall with a relatively large surface area and Tyr¹⁵⁷ and Phe²²⁹ take possession of the other side of the substrate-binding pocket. A hydrophobic region in the bottom side of the pocket was maintained by Leu³⁰⁰, Trp³⁰⁶, Met³¹¹, His³²⁸, Ser³²⁹, Gly³³⁰, Leu³⁵⁷, and Ile³⁵⁸. A small $\beta 5$ strand having a conserved H³²⁸-S³²⁹-G³³⁰ motif (Motif III) forms the lower

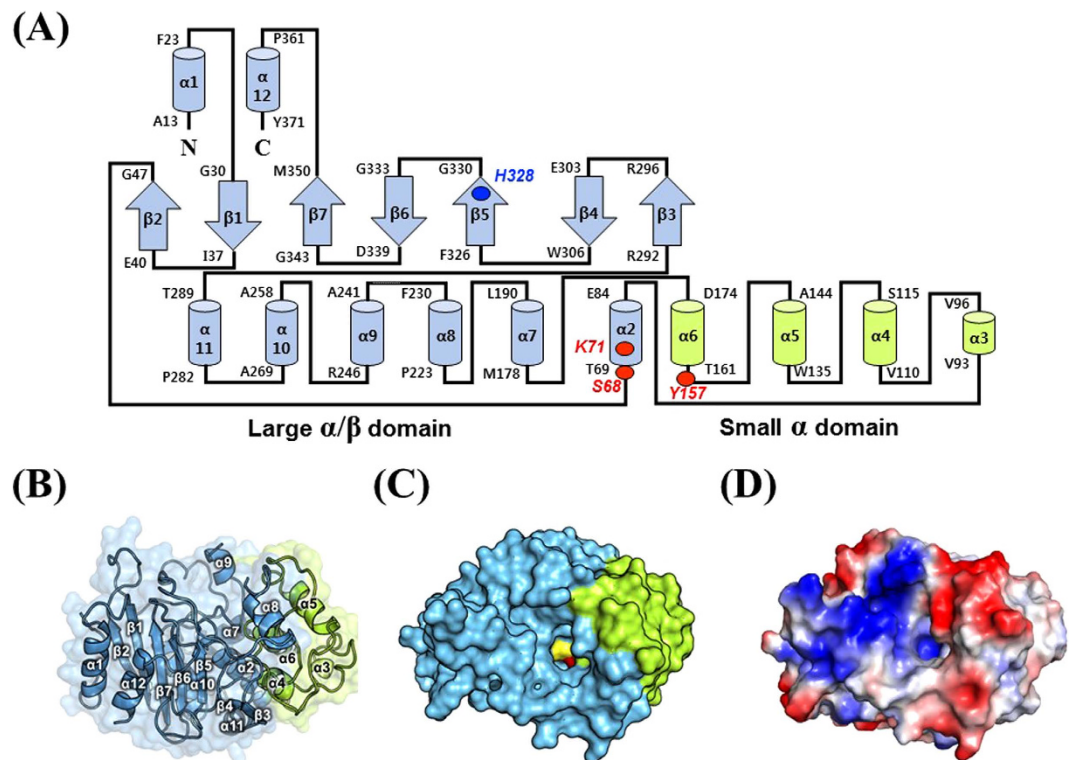


Figure 8. Structural visualization and topology diagram of CcEstA. The large α/β domain and small α domain of CcEstA are distinguished by different colors (light blue and light green, respectively). (A) Topology diagram of CcEstA. The catalytic triad residues are shown in red, and His³²⁸ in blue. The dashed line between $\alpha 8$ and $\alpha 9$ represents a missing invisible region of electron density. (B) The overall structure of CcEstA is shown with a ribbon diagram. (C) Molecular surface of CcEstA. The substrate-binding pocket of CcEstA is shown at the center. Inside the pocket, the catalytic Ser and Tyr are shown in yellow and red, respectively. (D) Surface charge distribution of CcEstA. Blue and red regions indicate local positive and negative charge, respectively.

end of the cleft. Two water molecules (W1 and W2) were observed in the substrate-binding pocket of CcEstA (Fig. 11B). A water molecule (W1) is anchored in the pocket by hydrogen-bonding interactions with Ser⁶⁸ and the main-chain nitrogen of Trp³³¹ from Motif III, which seems to be necessary for the efficient deacylation of substrates. Another water molecule (W2) at the other side of the catalytic residues stabilizes the $\alpha 8$ helix through hydrogen bonds with Ala²²⁸ and Ser²³⁴. Similar roles of water molecules are also observed in OXA-58 Class D β -lactamase³⁶.

As shown in Fig. 12, two extensive stretches of upper loop (UL: Gly¹⁹¹–Thr²⁵⁷) and lower loop (LL: Ala²⁹⁰–Ala³⁰⁸) over the active site constitute the entrance region for the substrate-binding pocket. The *B*-factor values of these regions were remarkably high compared to those of other regions, indicating that the conformational flexibility of these regions may be important for substrate binding. Specifically, *B*-factor values for this region of CcEstA were 26.7 \AA^2 (UL) and 22.1 \AA^2 (LL) for the main chain, and 27.4 \AA^2 (UL) and 27.4 \AA^2 (LL) for side chains, which are larger than the average *B*-factors of main-chain atoms (22.3 \AA^2) and side-chain atoms (22.1 \AA^2). In addition, the upper loop region ($\alpha 8/\alpha 9$ loop), flanked by $\alpha 8$ and $\alpha 9$ in CcEstA, makes few contacts with the rest of the protein, which may explain the conformational flexibility that is necessary for substrate binding and structural reorganization. The lower loop region of the $\beta 3/\beta 4$ loop, which projects towards the $\alpha 7/\alpha 8$ loop of the upper loop, wraps around catalytic residues and partially forms part of the substrate-binding site. However, in R61 DD-peptidase, the corresponding loop folds away from the active site, which enables large substrates to come into the substrate-binding pocket. Furthermore, the corresponding region in PaPBP is fully made up of flexible loops without any intervening β -strands. Therefore, accessibility toward the substrate-binding pocket of CcEstA is significantly more restricted than in R61 DD-peptidase and PaPBP. Differences in substrate specificity among these enzymes can be explained on the basis of their structural differences in this region. Interestingly, PBPs are known to have the ability to make large structural changes from quantum mechanics/molecular mechanics calculations³⁷ or structural and functional analysis^{38–41}. In accordance, changes in length, sequence, and conformation of loops around active sites are supposed to play a key role in the divergence of enzyme function^{42,43}.

In summary, a novel paralog (CcEstA) of PBPs from *Caulobacter crescentus* CB15 was characterized using biochemical analysis including native-PAGE, mass spectrometry, gel filtration, CD spectroscopy, fluorescence, reaction kinetics, and enzyme. CcEstA was shown to hydrolyze preferentially short-chain p-nitrophenyl esters, naphthyl esters, tertiary alcohol esters, and β -lactam nitrocefin. In addition, CcEstA structure revealed the flexibility in the substrate-binding pocket with two large loops of UL and LL. Structural and functional features of

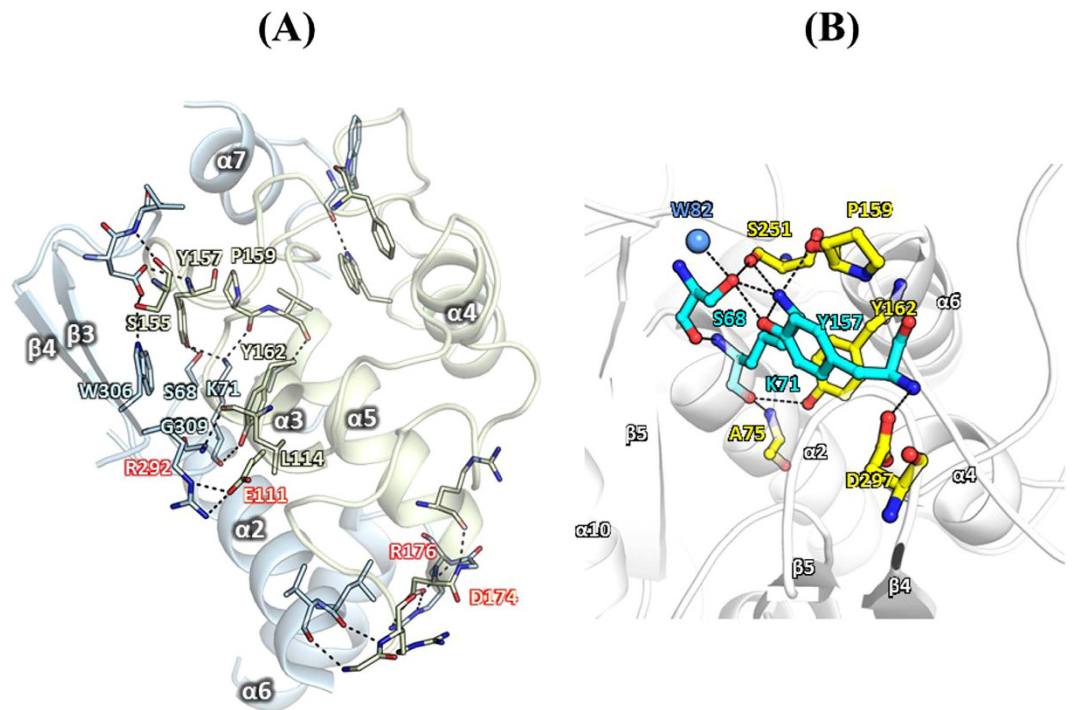


Figure 9. Domain-domain interfaces and hydrogen-bonding networks in the active site of CcEstA. (A) The interfaces between the large α/β domain (light blue) and the small α domain (light green) are shown. Electrostatic interactions and hydrogen bonds are shown with dashed lines. (B) The hydrogen-bonding network of CcEstA around the active site is shown.

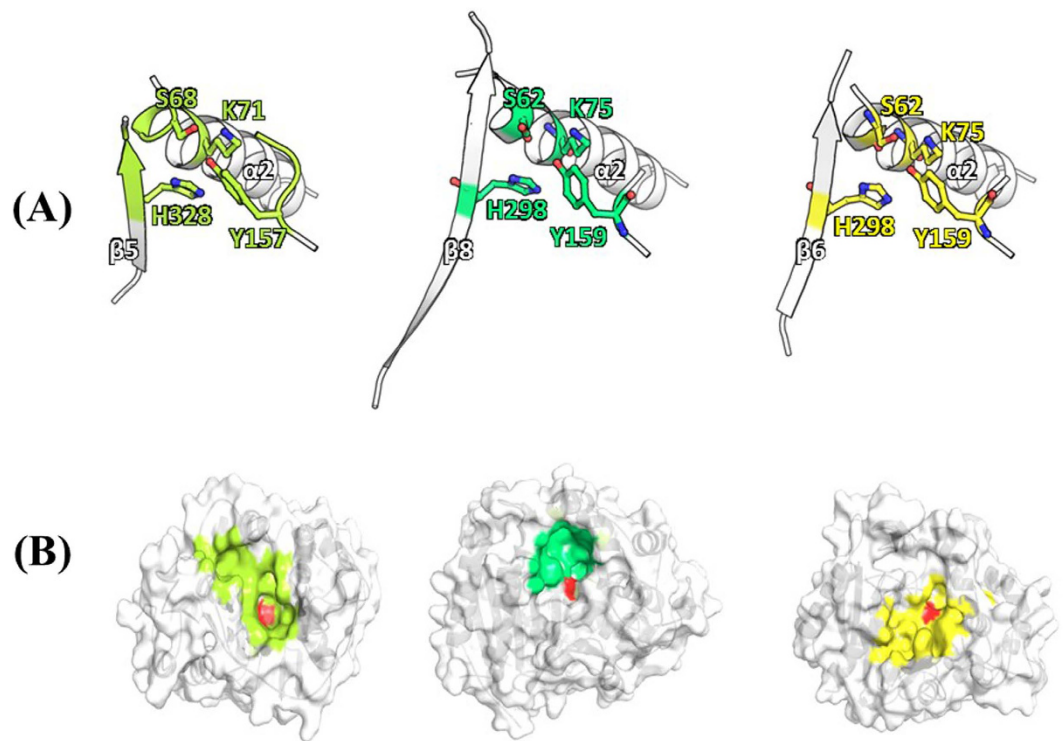


Figure 10. Comparison of the active site of CcEstA, R61 DD-peptidase (3PTE), and PaPBP (2QMI). (A) Ribbon diagram of enzyme active sites. Key residues (Ser and Lys in motif I, Tyr in motif II, and Histidine in motif III) in the active site are highlighted and shown as ball-and-stick model. (B) Molecular surfaces of the enzyme active site. Nucleophilic Ser is shown in red and other highly conserved residues (Lys, Tyr, and His) in the same color scheme with (A).

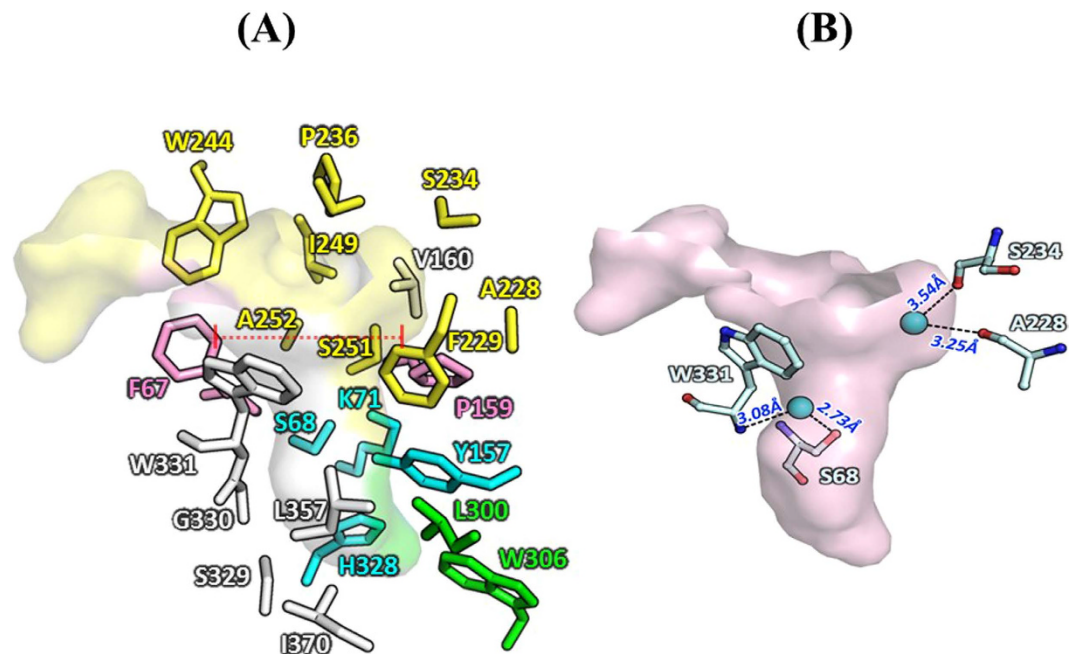


Figure 11. Substrate-binding pocket of CcEstA. (A) All residues forming the pocket are shown as a ball-and-stick model. Key residues of the active site are colored in cyan, the residues of UL in yellow, LL in green, and others in white. Two bulky residues of F67 and P159 are shown in purple and roof regions were indicated as a dotted line. (B) Four residues with two water molecules around the pocket of CcEstA are shown.

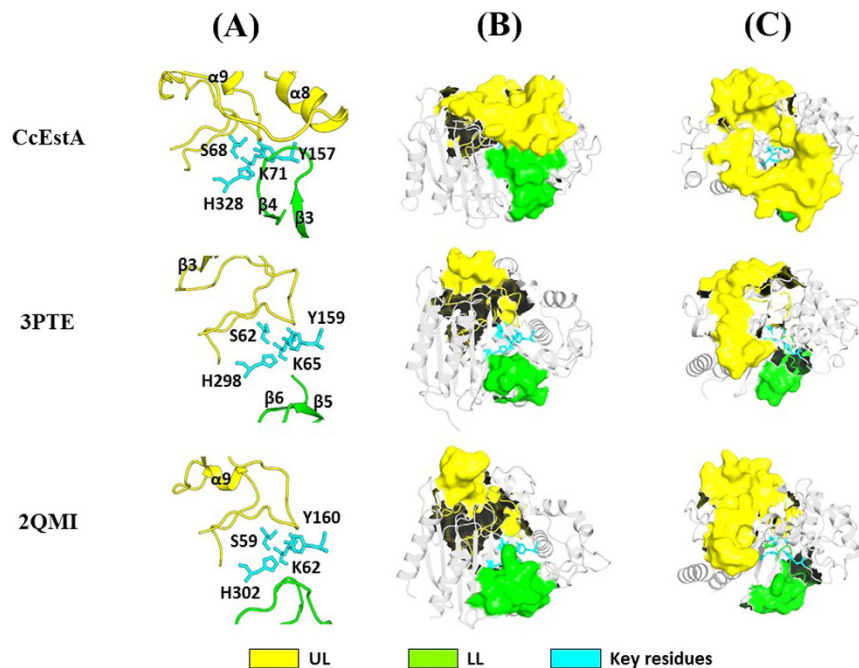


Figure 12. Analysis of UL and LL in CcEstA, R61 DD-peptidase (3PTE), and PaPBP (2QMI). (A) Catalytic residues are colored in cyan. The residues of UL are in yellow and those of LL are in green. (B,C) Molecular surface representation of UL and LL in ribbon diagram. Front view (B) and top view (C) are shown. Note that the orientation of UL and LL in CcEstA is different from those of R61 DD-peptidase (3PTE) and PaPBP (2QMI).

CcEstA derived from this analysis will provide a starting point for a comprehensive understanding of catalytic and structural features of PBP family and for the design of a novel class of antibiotics targeting PBP families. Although the role of CcEstA in peptidoglycan biosynthesis needs still to be explored, this protein might be involved in the

remodeling of peptidoglycan structure with its hydrolyzing activity. Further crystallographic analysis of CcEstA complexed with chemical ligands, mutagenesis of key residues, and in-depth kinetic analysis are necessary for a thorough understanding the substrate recognition mechanism of this enzyme.

Materials and Methods

Gene cloning and protein purification. Cloning and expression of CcEstA were performed as previously described¹⁷. Briefly, the CcEstA gene was PCR-amplified from chromosomal DNA of *C. Crescentus* CB15 (Microbank of Microbial Genomics and Application Center, Daejeon, Republic of Korea). The resulting PCR product was inserted into a pQE30 vector, where 12 additional codons encoding a His-tag (MRGSHHHHHHGS) were placed in frame at the N-terminal region. The construct was overexpressed in *Escherichia coli* XL1-Blue cells upon induction with 1 mM IPTG at 37 °C for 4 h. The harvested cells were lysed by sonication in lysis buffer (20 mM Tris-HCl pH 8.0, 100 mM NaCl). The lysate was centrifuged and the supernatant was loaded onto a His-Trap column (GE Healthcare). The column was washed with 5 column volumes of lysis buffer containing 40 mM imidazole. The protein was then eluted with lysis buffer containing 200 mM imidazole and desalted on a PD-10 column (GE Healthcare) with 50 mM Tris-HCl pH 8.0. The purified CcEstA was concentrated to 1 mg/mL in 50 mM Tris-HCl pH 8.0 using Vivaspin concentrators (GE Healthcare) without cleaving the N-terminal His-tag. The purity of the CcEstA was confirmed by SDS-PAGE and protein concentration was determined by the Bradford method (Bio-Rad, USA).

Biochemical assays of CcEstA. The esterase activity of CcEstA was determined mainly with *p*-nitrophenyl esters by measuring the absorbance at 405 nm using an EPOCH2 microplate reader (Biotek), as described previously¹⁷. The standard assay solution consisted of 250 μM substrate solution in 20 mM Tris-HCl pH 8.0 with 10 μg CcEstA protein (at a final concentration of ~800 nM). The naphthyl-group derivatives 1-naphthyl acetate (1-NA), 1-naphthyl butyrate (1-NB), 2-naphthyl acetate (2-NA), and 1-naphthyl phosphate (1-NP) were also used as substrates for analyzing regioselectivity, and the absorbance was determined at 310 nm under the same condition as described above.

Thermostability of CcEstA was measured by incubating the enzyme at 20 °C, 30 °C, 40 °C, 50 °C, and 60 °C for 1 h. Then, each aliquot was properly taken every 15 min for measuring the residual activity. The pH stability of CcEstA was examined by measuring catalytic activity in the pH range of 4.0–11.0. The buffer systems included citrate-NaOH (pH 3.0–6.0), phosphate-NaOH (pH 7.0), Tris-HCl (pH 8.0), and glycine-NaOH buffer (pH 9.0–11.0). To examine the effects of chemicals, CcEstA was incubated with each compound for 1 h at 25 °C, and the residual activity was determined using 10 mM *p*-nitrophenyl acetate (pNA) as a substrate.

For enantioselectivity analysis, CcEstA was incubated with either (*R*)- or (*S*)-solutions⁴⁴. The (*R*)- and (*S*)-solutions consisted of phenol red (1 mg/mL), 20 mM Tris-HCl pH 8.0 and 300 mM methyl-(*R*)-(-)-3-hydroxy-2-methylpropionate or methyl-(*S*)-(+)-3-hydroxy-2-methylpropionate solution. This pH indicator-based colorimetric assay was also performed to verify the activity of CcEstA toward cefotaxime (CTX) and 7-aminocephalosporanic acid (7-ACA), respectively. CcEstA was incubated with 12 mM CTX or 7-ACA at 25 °C for 1 h. The β-lactamase activity of CcEstA was determined using a chromogenic β-lactam substrate, nitrocefin [2*S*,5*R*,6*R*]-6-[[carboxy(phenyl)acetyl]amino]-3,3-dimethyl-7-oxo-4-thia-1-azabicyclo[3.2.0]heptane-2-carboxylic acid. CcEstA (0.5 mg/ml) was reacted with a 484 μM nitrocefin solution in 20 mM Tris-HCl pH 8.0 at 25 °C, and the color change in the reaction mixture was observed.

Mass spectrometry, CD spectroscopy, and fluorescence analysis. Matrix-assisted laser desorption/ionization time-of-flight mass spectrometry was performed with a Voyager DE STR system in positive-ion mode⁴⁴. For an overlay activity assay, native-PAGE was performed and the gel was rinsed several times with 50 mM sodium phosphate buffer at pH 7.0. Then, 0.25 mM 4-methylumbelliferyl (4-MU) acetate was added to detect blue fluorescence under UV illumination, which is emitted from 4-MU after hydrolysis⁴⁵. The molecular mass of CcEstA was estimated by gel filtration FPLC (AKTA UPC-900, GE Healthcare) on a Superdex 200GL column (GE Healthcare).

Circular dichroism (CD) spectra were recorded with a Jasco J715 spectropolarimeter with a Peltier temperature control (Jasco, MD, U.S.A.) Far-UV CD analysis were carried out in the wavelength range of 190 to 260 nm with a 0.5 nm bandwidth, 1 s response time, and 200 nm/min scan speed. All spectra were corrected by the subtraction of the buffer signal. The raw CD signal, θ , was converted to mean residue ellipticity using the equation $[\theta]_{MRW} = \theta / (10C_r l)$, where C_r represents the concentration and l is the path length. For thermal unfolding analysis, the CD signal was monitored at 222 nm using a 0.1 cm path length at a scan rate of 1 °C/min with 1 mg/ml CcEstA.

All fluorescence measurements were carried out using a Jasco FP-6200 spectrofluorometer (Jasco, MD, U.S.A.). Urea-induced unfolding of CcEstA was performed by incubating the protein with various concentrations of urea at 25 °C for 1 h. Protein samples were excited at 290 nm, and the emission spectra were recorded in the range of 300 to 400 nm. All fluorescence spectra were recorded with a scan speed of 250 nm/min with a 5 nm slit width.

Kinetic assays. Kinetic assays were performed using *p*-NA, *p*-NO, and nitrocefin as substrates. Enzyme solutions were prepared in 20 mM Tris-HCl pH 8.0 buffer. The enzyme concentrations differed between *p*-nitrophenyl esters and nitrocefin reactions (40 nM or 15 μM of CcEstA, respectively). Various concentrations of substrate were added to the enzyme solutions. The reactions were performed at RT, and monitored using the EPOCH2 microplate reader (Biotek) at 405 nm for *p*-nitrophenyl esters, and at 486 nm for nitrocefin. Measurements were taken every 10 s for 15 min (1 min for 5 h with nitrocefin). Each concentration of substrate was measured along with a blank and at least 3 measurements were collected to determine the rate. Sample path-length correction was done automatically by Gen5 software (Biotek, USA). The molar extinction coefficients of *p*-nitrophenol and

nitrocefin were determined experimentally (*p*-nitrophenol: 17,154 M⁻¹ cm⁻¹, and nitrocefin: 12,124 M⁻¹ cm⁻¹). The reaction velocities were determined from the initial linear portion of the progress curves, which were generated after subtracting absorbance of the blank, correcting sample path-length, and converting absorbance into product concentration [P] with the experimentally obtained extinction coefficient. From the *x*- and *y*-intercepts of the Lineweaver-Burk plot, parameters of V_{\max} and K_m were obtained for each substrate. The k_{cat} was calculated using the equation $k_{\text{cat}} = V_{\max}/[E]_t$.

Crystallization and X-ray Data collection. Crystallization was performed using the microbatch crystallization method under a thin layer of Al's oil, using the commercially available screening kits Wizard I, II (Emerald BioSystems, Washington, USA) and Crystal Screen I, II (Hampton Research, CA, USA) at 295 K. Diffraction-quality crystals were obtained from the condition Wizard I-34 (1.0 M ammonium phosphate dibasic, 0.1 M imidazole pH 8.0) and Crystal Screen I-42 (50 mM potassium phosphate monobasic, 20% w/v polyethylene glycol 8000). Crystals were immediately frozen in a cold nitrogen stream for MAD data collection. For X-ray data collection, the CcEstA crystal was transferred in the cryosolvent containing the same reservoir and 20% glycerol before being flash-frozen in a cold nitrogen stream. X-ray diffraction data were collected at 100 K using an ADSC Quantum 315 CCD on beamline PAL 4 A at the Pohang Accelerator Laboratory (PAL), Korea. The data were indexed, integrated and scaled using HKL-2000. The data collection and processing statistics are summarized in Table 1.

Structure determination and refinement. The structure of CcEstA was solved by MOLREP⁴⁶ using the molecular replacement method using the crystal structure of EstA from *Arthrobacter nitroguajacolicus* Rue61a (PDB 3ZYT) as a template. The automated model building was performed by PHENIX Autobuild. The model was refined many steps using REFMAC⁴⁷ and PHENIX⁴⁸. The quality of the final model was evaluated with the program MOLPROBITY⁴⁹. Refinement statistics are given in the Table 1.

Sequence and structure analysis. To identify related enzymes in the PBP family, protein data bank (PDB) was searched for sequences similar to the primary sequence of CcEstA. All primary sequences were retrieved from Swiss-Prot in FASTA format⁵⁰. Multiple sequence alignments were performed using Clustal Omega⁵¹ and the results were rendered using ESPrict⁵². The enzymes possessing structural similarity to CcEstA were found using the DALI server⁵³. Two related proteins (R61 DD-peptidase from *Streptomyces* R61 and PaPBP from *Pyrococcus abyssi*) that were found in both BLAST and DALI searches, were selected for structural comparison with CcEstA. Superposition of the enzymes was performed using CCP4 software⁵⁴. PyMOL v1.8 was used to represent three-dimensional structures of the enzymes (PyMOL Molecular Graphics System, Schrödinger, LLC). Coordinates and structure factors have been deposited in the RCSB Protein Data Bank as accession number 5GKV.

References

1. Lovering, A. L., Safadi, S. S. & Strynadka, N. C. Structural perspective of peptidoglycan biosynthesis and assembly. *Annu. Rev. Biochem.* **81**, 451–478 (2012).
2. Scheurwater, E. M. & Burrows, L. L. Maintaining network security: how macromolecular structures cross the peptidoglycan layer. *FEMS Microbiol. Lett.* **318**, 1–9 (2011).
3. Typas, A., Banzhaf, M., Gross, C. A. & Vollmer, W. From the regulation of peptidoglycan synthesis to bacterial growth and morphology. *Nat. Rev. Microbiol.* **10**, 123–136 (2011).
4. Frère, J. M. & Page, M. G. Penicillin-binding proteins: evergreen drug targets. *Curr. Opin. Pharmacol.* **18**, 112–119 (2014).
5. Spratt, B. G. The 2011 Garrod Lecture: From penicillin-binding proteins to molecular epidemiology. *J. Antimicrob. Chemother.* **67**, 1578–1588 (2012).
6. Macheboeuf, P., Contreras-Martel, C., Job, V., Dideberg, O. & Dessen, A. Penicillin binding proteins: key players in bacterial cell cycle and drug resistance processes. *FEMS Microbiol. Rev.* **30**, 673–691 (2006).
7. Sauvage, E., Kerff, F., Terrak, M., Ayala, J. A. & Charlier, P. The penicillin-binding proteins: structure and role in peptidoglycan biosynthesis. *FEMS Microbiol. Rev.* **32**, 234–258 (2008).
8. Tsokos, C. G. & Laub, M. T. Polarity and cell fate asymmetry in *Caulobacter crescentus*. *Curr. Opin. Microbiol.* **15**, 744–750 (2012).
9. Curtis, P. D. & Brun, Y. V. Getting in the loop: regulation of development in *Caulobacter crescentus*. *Microbiol. Mol. Biol. Rev.* **74**, 13–41 (2010).
10. Strobel, W., Möll, A., Kiekebusch, D., Klein, K. E. & Thanbichler, M. Function and localization dynamics of bifunctional penicillin-binding proteins in *Caulobacter crescentus*. *J. Bacteriol.* **196**, 1627–1639 (2014).
11. Hughes, H. V. *et al.* Co-ordinate synthesis and protein localization in a bacterial organelle by the action of a penicillin-binding-protein. *Mol. Microbiol.* **90**, 1162–1177 (2013).
12. Jeon, J. H. *et al.* Novel metagenome-derived carboxylesterase that hydrolyzes β -lactam antibiotics. *Appl. Environ. Microbiol.* **77**, 7830–7836 (2011).
13. Mokoena, N., Mathiba, K., Tsekoa, T., Steenkamp, P. & Rashamuse, K. Functional characterisation of a metagenome derived family VIII esterase with a deacetylation activity on β -lactam antibiotics. *Biochem. Biophys. Res. Commun.* **437**, 342–348 (2013).
14. Yu, E. Y. *et al.* Isolation and characterization of cold-active family VIII esterases from an arctic soil metagenome. *Appl. Microbiol. Biotechnol.* **90**, 573–581 (2011).
15. Rashamuse, K., Magomani, V., Ronneburg, T. & Brady, D. A novel family VIII carboxylesterase derived from a leachate metagenome library exhibits promiscuous beta-lactamase activity on nitrocefin. *Appl. Microbiol. Biotechnol.* **83**, 491–500 (2009).
16. Ryu, B. H. *et al.* Identification, crystallization and preliminary X-ray diffraction analysis of esterase A from *Caulobacter crescentus* CB15, a family VIII lipolytic enzyme. *Acta Crystallogr. Sect. F Struct. Biol. Cryst. Commun.* **68**, 560–564 (2012).
17. Peitsaro, N. *et al.* Evolution of a family of metazoan active-site-serine enzymes from penicillin-binding proteins: a novel facet of the bacterial legacy. *BMC Evol. Biol.* **8**, 26 (2008).
18. Goffin, C. & Ghuyssen, J. M. Multimodular penicillin-binding proteins: an enigmatic family of orthologs and paralogs. *Microbiol. Mol. Biol. Rev.* **62**, 1079–1093 (1998).
19. Pratt, R. F. & McLeish, M. J. Structural relationship between the active sites of β -lactam-recognizing and amidase signature enzymes: convergent evolution? *Biochemistry* **49**, 9688–9697 (2010).

20. McDonough, M. A. *et al.* Structures of two kinetic intermediates reveal species specificity of penicillin-binding proteins. *J. Mol. Biol.* **322**, 111–122 (2002).
21. Okazaki, S. *et al.* Crystal structure and functional characterization of a D-stereospecific amino acid amidase from *Ochrobactrum anthropi* SV3, a new member of the penicillin-recognizing proteins. *J. Mol. Biol.* **368**, 79–91 (2007).
22. Oh, C. *et al.* Structural and Biochemical Characterization of an Octameric Carbohydrate Acetyltransferase from *Sinorhizobium meliloti*. *FEBS Lett.* **590**, 1242–1252 (2016).
23. Ngo, T. D. *et al.* Crystallographic analysis and biochemical applications of a novel penicillin-binding protein/ β -lactamase homologue from a metagenomic library. *Acta Crystallogr. D. Biol. Crystallogr.* **70**, 2455–2466 (2014).
24. Jeong, J. H. *et al.* Crystal structures of bifunctional penicillin-binding protein 4 from *Listeria monocytogenes*. *Antimicrob. Agents. Chemother.* **57**, 3507–3512 (2013).
25. King, D. T., Lameignere, E. & Strynadka, N. C. Structural insights into the lipoprotein outer membrane regulator of penicillin-binding protein 1B. *J. Biol. Chem.* **289**, 19245–19253 (2014).
26. Yoshida, H. *et al.* Crystal structures of penicillin-binding protein 3 (PBP3) from methicillin-resistant *Staphylococcus aureus* in the apo and cefotaxime-bound forms. *J. Mol. Biol.* **423**, 351–364 (2012).
27. Krissinel, E. & Henrick, K. Inference of macromolecular assemblies from crystalline state. *J. Mol. Biol.* **372**, 774–797 (2007).
28. Kim, K. *et al.* Structural and biochemical characterization of a carbohydrate acetyltransferase from *Sinorhizobium meliloti* 1021. *FEBS Lett.* **589**, 117–122 (2015).
29. Greenfield, N. J. Using circular dichroism spectra to estimate protein secondary structure. *Nat. Protoc.* **1**, 2876–2890 (2006).
30. Ngo, T. D. *et al.* Crystallographic analysis and biochemical applications of a novel penicillin-binding protein/ β -lactamase homologue from a metagenomic library. *Acta Crystallogr. D. Biol. Crystallogr.* **70**, 2455–2466 (2014).
31. Kourist, R. & Bornscheuer, U. T. Biocatalytic synthesis of optically active tertiary alcohols. *Appl. Microbiol. Biotechnol.* **91**, 505–517 (2011).
32. Sainsbury, S. *et al.* Crystal structures of penicillin-binding protein 3 from *Pseudomonas aeruginosa*: comparison of native and antibiotic-bound forms. *J. Mol. Biol.* **405**, 173–184 (2011).
33. Chen, Y. *et al.* Crystal structures of penicillin-binding protein 6 from *Escherichia coli*. *J. Am. Chem. Soc.* **131**, 14345–14354 (2009).
34. Lovering, A. L., de Castro, L. H., Lim, D. & Strynadka, N. C. Structural insight into the transglycosylation step of bacterial cell-wall biosynthesis. *Science*. **315**, 1402–1405 (2007).
35. Fisher, J. F., Meroueh, S. O. & Mobashery, S. Bacterial resistance to beta-lactam antibiotics: compelling opportunism, compelling opportunity. *Chem. Rev.* **105**, 395–424 (2005).
36. Pratap, S., Katiki, M., Gill, P., Kumar, P. & Golemi-Kotra, D. Active-site plasticity is essential to carbapenem hydrolysis by OXA-58 class D β -lactamase of *Acinetobacter baumannii*. *Antimicrob. Agents Chemother.* **60**, 75–86 (2015).
37. Shi, Q., Meroueh, S. O., Fisher, J. F. & Mobashery, S. Investigation of the mechanism of the cell wall DD-carboxypeptidase reaction of penicillin-binding protein 5 of *Escherichia coli* by quantum mechanics/molecular mechanics calculations. *J. Am. Chem. Soc.* **130**, 9293–9303 (2008).
38. Nakano, S. *et al.* Structural and computational analysis of peptide recognition mechanism of class-C type penicillin binding protein, alkaline D-peptidase from *Bacillus cereus* DF4-B. *Sci. Rep.* **5**, 13836 (2015).
39. Petrella, S. *et al.* Genetic and structural insights into the dissemination potential of the extremely broad-spectrum class A beta-lactamase KPC-2 identified in an *Escherichia coli* strain and an *Enterobacter cloacae* strain isolated from the same patient in France. *Antimicrob. Agents Chemother.* **52**, 3725–3736 (2008).
40. Kotsakis, S. D. *et al.* Interactions of oximino-substituted boronic acids and β -lactams with the CMY-2-derived extended-spectrum cephalosporinases CMY-30 and CMY-42. *Antimicrob. Agents. Chemother.* **57**, 968–976 (2013).
41. Contreras-Martel, C. *et al.* PBP active site flexibility as the key mechanism for beta-lactam resistance in pneumococci. *J. Mol. Biol.* **387**, 899–909 (2009).
42. Afriat-Jurnou, L., Jackson, C. J. & Tawfik, D. S. Reconstructing a missing link in the evolution of a recently diverged phosphotriesterase by active-site loop remodeling. *Biochemistry* **51**, 6047–6055 (2012).
43. Tawfik, D. S. Loop grafting and the origins of enzyme species. *Science*. **311**, 475–476 (2006).
44. Ngo, T. D. *et al.* Crystallographic analysis and biochemical applications of a novel penicillin-binding protein/ β -lactamase homologue from a metagenomic library. *Acta Crystallogr. D. Biol. Crystallogr.* **70**, 2455–2466 (2014).
45. Jang, E. *et al.* Preparation of cobalt nanoparticles from polymorphic bacterial templates: A novel platform for biocatalysis. *Int. J. Biol. Macromol.* **81**, 747–753 (2015).
46. Adams, P. D. *et al.* PHENIX: a comprehensive Python-based system for macromolecular structure solution. *Acta Crystallogr D Biol Crystallogr.* **66**, 213–221 (2010).
47. Vagin, A. & Teplyakov, A. Molecular replacement with MOLREP. *Acta Crystallogr D Biol Crystallogr.* **66**, 22–25 (2010).
48. Murshudov, G. N. *et al.* REFMAC5 for the refinement of macromolecular crystal structures. *Acta Crystallogr. D. Biol. Crystallogr.* **67**, 355–367 (2011).
49. Chen, V. B. *et al.* MolProbity: all-atom structure validation for macromolecular crystallography. *Acta Crystallogr. D. Biol. Crystallogr.* **66**, 12–21 (2010).
50. Artimo, P. *et al.* ExPASy: SIB bioinformatics resource portal. *Nucleic Acids Res.* **40**, W597–603 (2012).
51. Sievers, F. *et al.* Fast, scalable generation of high-quality protein multiple sequence alignments using Clustal Omega. *Mol. Syst. Biol.* **7**, 539 (2011).
52. Gouet, P., Robert, X. & Courcelle, E. ESPript/ENDscript: Extracting and rendering sequence and 3D information from atomic structures of proteins. *Nucleic Acids Res.* **31**, 3320–3323 (2003).
53. Holm, L. & Rosenström, P. Dali server: conservation mapping in 3D. *Nucleic Acids Res.* **38**, W545–549 (2010).
54. Winn, M. D. *et al.* Overview of the CCP4 suite and current developments. *Acta Crystallogr. D. Biol. Crystallogr.* **67**, 235–242 (2011).
55. Kim, Y. O. *et al.* A novel esterase from *Paenibacillus* sp. PBS-2 is a new member of the β -lactamase belonging to the family VIII lipases/esterases. *J. Microbiol. Biotechnol.* **24**, 1260–1268 (2014).

Acknowledgements

We are grateful to Dr. Gergely Toth (University of Cambridge, U.K) for his help in this project. This study was supported by a grant of the Korean Health Technology R&D Project, Ministry of Health & Welfare, Republic of Korea (HI14C2315) to T.D.K., and Next-Generation BioGreen 21 Program (SSAC PJ001107005), and the National Research Foundation of Korea (NRF) grant (2016R1A2B2008081) to K.K.

Author Contributions

B.H.R. and T.D.K. identified the gene from the chromosome of *C. Crescentus* CB15. B.H.R., S.L., and T.D.N. overexpressed and crystallized the protein. The protein was biochemically characterized by B.H.R., W.Y., S.L., B.K., E.L., and T.D.N. The structure was determined by T.D.N. and K.K.K. T.D.K. and K.K.K. coordinated the project and wrote the manuscript. All authors reviewed the results and approved the final version of the manuscript.

Additional Information

Accession codes: The coordinates and structure factors for CcEstA have been deposited in the Protein Data Bank with code: 5GKV.

Supplementary information accompanies this paper at <http://www.nature.com/srep>

Competing financial interests: The authors declare no competing financial interests.

How to cite this article: Ryu, B. H. *et al.* Biochemical and Structural Analysis of a Novel Esterase from *Caulobacter crescentus* related to Penicillin-Binding Protein (PBP). *Sci. Rep.* **6**, 37978; doi: 10.1038/srep37978 (2016).

Publisher's note: Springer Nature remains neutral with regard to jurisdictional claims in published maps and institutional affiliations.



This work is licensed under a Creative Commons Attribution 4.0 International License. The images or other third party material in this article are included in the article's Creative Commons license, unless indicated otherwise in the credit line; if the material is not included under the Creative Commons license, users will need to obtain permission from the license holder to reproduce the material. To view a copy of this license, visit <http://creativecommons.org/licenses/by/4.0/>

© The Author(s) 2016